PROCEEDINGS of the
24th International Congress on Acoustics

October 24 to 28, 2022 in Gyeongju, Korea

ABS-0243

Modeling and measurements of organ pipe sound radiation

Samuel D. BELLOWS[1]; Timothy W. LEISHMAN[2]

[1,2] Brigham Young University, USA

ABSTRACT

Pipe organs have played an important role in Western musical genres for centuries and are unique in their acoustic radiation as sound is produced from numerous pipes. At low frequencies, the directivity of an individual organ pipe can be roughly modeled using one or two point sources, whose source strengths can be determined, for example, using transmission matrix methods. This work studies the limitations of this approach in predicting the directivities of organ pipes at higher frequencies involving diffraction effects. Modeled directivities are compared to those measured with a spherical array and with a near-field cylindrical array to illustrate the differences.

Keywords: Directivity

1. INTRODUCTION

The transmission matrix method (TMM) represents a complex system as a one-dimensional transmission line, allowing a simple yet robust approach to modeling many musical instruments (1). Because the one-dimensional model is approximately valid as long as the instrument bore remains small compared to the acoustic wavelength, this approach is particularly useful in predicting the frequencies produced using various fingerings of wind instruments even for higher frequencies. While it is common to utilize the TMM to predict played frequencies and input impedance curves, the approach also helps predict the directional characteristics of musical instruments. Nonetheless, the effectiveness of the TMM in predicting directivities have remained inconclusive, partly due to the lack of high spatial resolution directivity measurements for comparisons.

This work contrasts TMM-based directivity models to measured spherical directivities. In particular, this investigation applies the TMM to organ pipes due to their simple natures. Results show that the TMM-based techniques successfully predict directivities at low frequencies. However, BEM simulations and near-field cylindrical scans reveal that the neglecting of diffraction effects limits the effectiveness of the approach.

2. THEORETICAL MODELING

At low frequencies, a simple point-source model reasonably describes the radiation of sound from the organ pipes (2, 3). For open pipes, two sources are necessary: one at the mouth and one at the open end. For a closed pipe, only a single source at the mouth is necessary. For time-harmonic radiation, the pressure at a point $\boldsymbol{r}$ is

$$p(\boldsymbol{r},k) = iz_0 k \sum_{n=1}^{N} U_n G(r,r_n)\,, \tag{1}$$

where N is the number of openings, U_n is the frequency-dependent volume velocity at the nth opening,

[1] samuel.bellows11@gmail.com
[2]tim_leishman@byu.edu

i is the imaginary unit, $z_0 = \rho_0 c$ is the characteristic specific acoustic impedance of the fluid, k is the wavenumber, and

$$G(r, r_n) = \frac{e^{-ikR_n}}{4\pi R_n} \tag{2}$$

is the free-space Green's function with

$$R_n = |\boldsymbol{r} - \boldsymbol{r_n}| \tag{3}$$

being the distance from the observation position $\boldsymbol{r}$ to the location $\boldsymbol{r_n}$ of the n^{th} opening.

When considering normalized far-field directivities, the volume velocity of the mouth is arbitrary for a closed pipe with only one opening. However, for an open pipe, the impedance translation theorem relates the volume velocity between the two openings (1, 3). The TMM simplifies the numerical implementation for more complex sources with many openings (3). The acoustic radiation impedance of the open end of the pipe can be modeled as an unflanged tube:

$$Z_{AR,O} = \frac{z_0}{S}(0.25(ka)^2 + i0.6ka). \tag{4}$$

The acoustic radiation impedance of the mouth can be roughly modeled as a baffled circular piston:

$$Z_{AR,M} = \frac{z_0}{S}\left(1 - \frac{J_1(2ka)}{ka} + \frac{iH_1(2ka)}{ka}\right). \tag{5}$$

Translating the impedance of the open end through length L to the mouth opening yields

$$Z_A = Z_{A0}\frac{Z_{AR,O} + iZ_{A0}\tan(kL)}{Z_{A0} + iZ_{AR,O}\tan(kL)}, \tag{6}$$

,

where $Z_{A0} = z_0/S$ and S is the pipe's cross-sectional area. A current divider circuit gives the volume velocity at the mouth as

$$U_m = U_{in}\frac{Z_A}{Z_A + Z_{AR,M}}, \tag{7}$$

where U_{in} is an arbitrary input volume velocity. Finally, the volume velocity at the end of the pipe is given by another current divider circuit:

$$U_O = (U_{in} - U_m)\frac{-iZ_{A0}\csc(kL)}{iZ_{A0}(\tan(kL/2) - \csc(kL)) + Z_{AR,O}}. \tag{8}$$

Thus, a simple model can estimate the volume velocities at the pipe openings for predicting far-field directivities using Eq. (1).

2.1 Kirchhoff-Helmholtz Integral Equation

A more complete representation of the pressure field follows from the Kirchhoff-Helmholtz Integral Equation (KHIE) (4):

$$p(r) = iz_0 k \iint u_n(r_s)G(r, r_s)dS + \iint p(r_s)\frac{\partial}{\partial n}G(r, r_s)dS, \tag{9}$$

where u_n is the normal particle velocity, the integral is taken over the boundary S and n is the normal direction into the domain. In this form, the first integral of the KHIE can be roughly interpreted as the radiation of sound from the source due to surface vibrations, whereas the second integral can be interpreted as the pressure field due to diffraction and scattering effects of the boundary.

If one considers the boundary surface S to fully enclose the exterior of the pipe, it is evident that

Eq. (1) approximates the first integral of the KHIE with

$$U_n = \iint u_n(r_s) dS_n, \tag{10}$$

where S_n is the surface bounding the n^{th} pipe opening. With this approach, the openings of the pipe behave as vibrating pistons of effective areas S_n. This approximation should remain valid provided that the acoustic wavelength is larger than the pipe openings. However, Eq. (1) neglects the second integral in the KHIE. Thus, when this term becomes important, deviations between the modeled and measured directivities will arise. Section 5 explores this limitation by comparing measured results with a BEM simulation, which numerically evaluates Eq. (9).

3. MEASUREMENTS

The authors employed spherical and cylindrical arrays to measure the pressure fields produced by two organ pipes: one open metal pipe and closed wood pipe. The spherical array, shown with the closed wooden pipe in Fig. 1(a), consisted of 36 12.7 mm (0.5 in) microphones placed in 5-degree increments in the polar angle at a radius of a = 0.97 m. The cylindrical array, shown with the open metal pipe in Fig. 1(b), consisted of 36 6.35 mm (0.25 in) microphones placed in 5 cm increments at a circular radius of ρ = 0.25 m. A turntable rotated each array in 5-degree azimuthal steps. Relative calibrations for each microphone array and a near-field reference microphone ensured normalization between the repeated measurements using frequency-response functions (FRFs) [(5)].

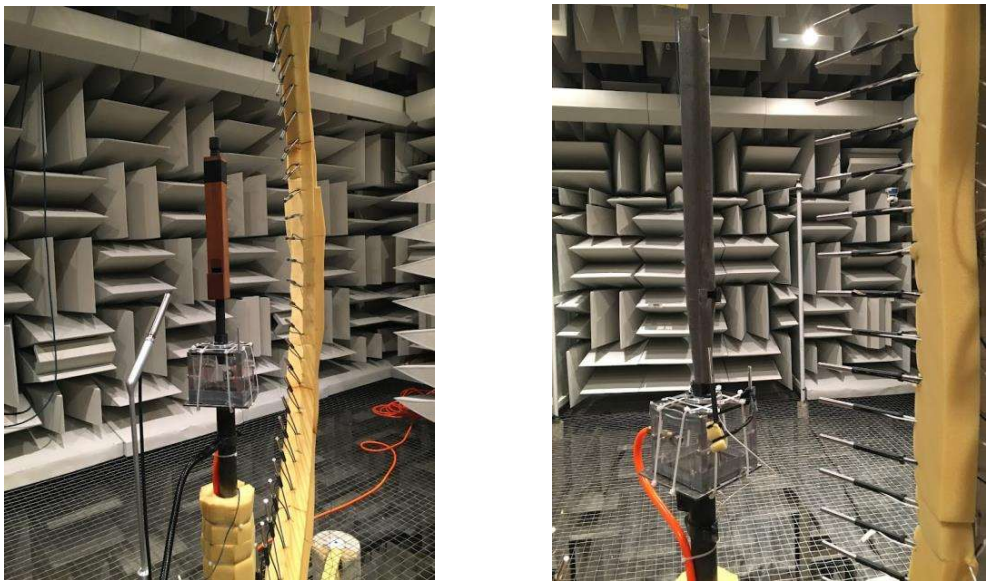

(a) (b)

Figure 1. Spherical (a) and cylindrical (b) microphone arrays used to assess the radiated fields of two organ pipes.

4. RESULTS

4.1 Theoretical Prediction

Figure 2 shows simulated directivity balloons for the first through sixth partials of the open metal pipe using Eq. (1) with L = 0.46 m. Both radius and color indicate levels on a 40 dB scale. The mouth of the pipe faces the $\phi = 0°$ azimuthal marker. For the fundamental, the directivity appears as a single disc-like shape. As anticipated for a two point-source model, as frequency increases, the number of lobes also increases. The directivity patterns are nearly axisymmetric about the line connecting the center of the top opening of the pipe with the mouth. Because the wooden pipe has only one radiating

opening, the simulated directivity pattern for all frequencies is omnidirectional.

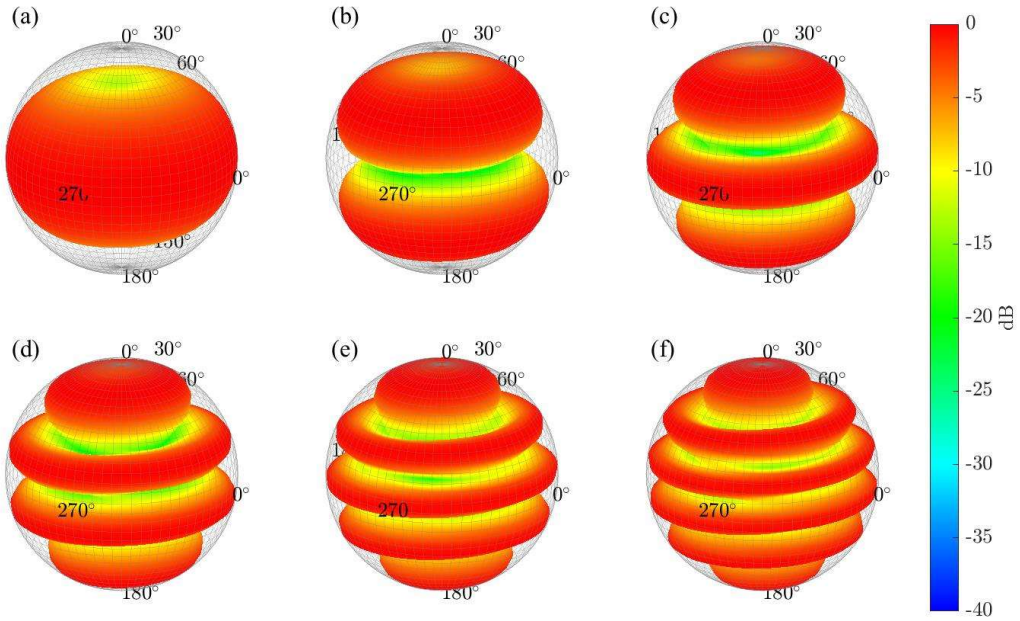

Figure 2. Simulated directivity balloons of the open metal pipe using Eq. (1) for the first six partials: (a) 331 Hz, (b) 662 Hz, (c) 993 Hz, (e) 1323 Hz, (f) 1654 Hz, and (f) 1985 Hz.

4.2 Directivity Measurements

Figure 3 shows the directivity balloons of the measured metal pipe. The patterns are remarkably similar, especially for the first three partials below 1 kHz. As for the simulated case, the balloons are roughly axisymmetric about the axis connecting the openings. However, at higher frequencies, reduced levels appear behind the pipe (near $\phi = 180°$) that reduce the axial symmetry.

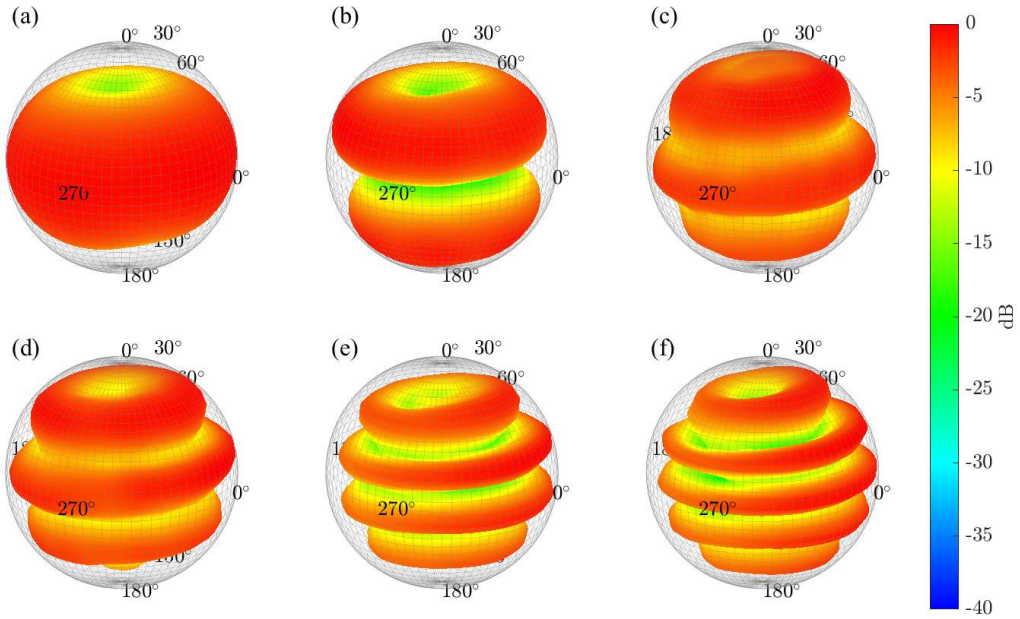

Figure 3. Measured directivity balloons of the open metal pipe for the first six partials: (a) 331 Hz, (b) 662 Hz, (c) 993 Hz, (e) 1323 Hz, (f) 1654 Hz, and (f) 1985 Hz.

Figure 4 shows the measured closed wooden pipe. While for the fundamental, the radiation is roughly omnidirectional, at higher frequencies, particularly above 1 kHz, the radiation is significantly reduced behind the instrument. Small undulations appear, although they are weak and not nearly as pronounced as for the open pipe.

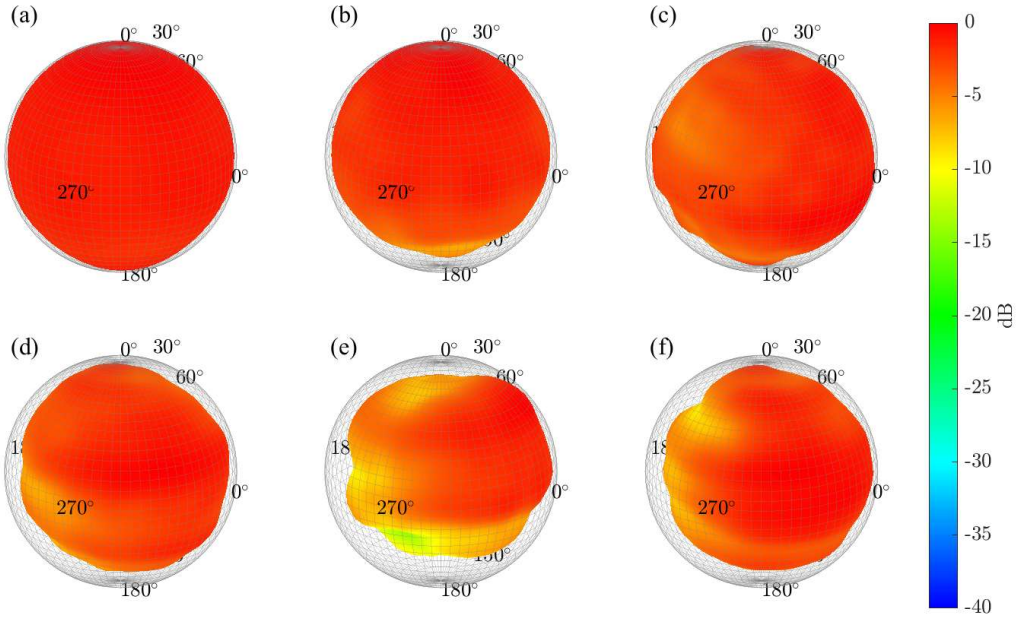

Figure 4. Measured directivity balloons for the measured closed wooden pipe for the first six partials: (a) 335 Hz, (b) 670 Hz, (c) 1005 Hz, (e) 1340 Hz, (f) 1675 Hz, and (f) 2010 Hz.

5. ANALYSIS

As suggested by the measurement results, simple point-source models provide reasonable estimates of source directivities at lower frequencies. However, reduced levels behind the pipes suggest that diffraction around the pipe itself may play an important role in the radiation patterns, particularly at higher frequencies. An enhanced model using a BEM evaluation of the KHIE provides additional insights into this assertion.

To simulate the pressure while maintaining similarity to the modeling approach used in Eq. (1), a single boundary enveloping the exterior of the pipe describes the source geometry. This approach divides the pipe into an exterior and interior portion so that the openings of the pipes become inhomogeneous Neumann (velocity) boundary conditions. Then, as shown in Eq. (10), the net volume velocity used in Eq. (1) is the surface integral of the particle velocity at each opening. The TMM method predicts the particle velocity at each opening by dividing the predicted values from Eqs. (7) and (8) by the area S_n of the opening. While a more accurate model would follow from treating the pipes as thin-walled structures and allowing the computational domain to include both the interior and exterior of the pipe, this method is useful because it maintains a consistent approach between the simple point-source model of Eq. (1) and the first term of the KHIE. The second term of the KHIE, numerically evaluated using BEM, can then be seen as a correction term to the original model.

Because the field produced by the second term decays at a faster rate than the $1/r$ dependence of the first term due to the normal derivative of the Green's function, this field is more apparent in the near-field of the source. Consequently, measurements produced by the cylindrical array are beneficial for identifying the effects of the second term in the KHIE.

Figure 5 plots results for the fundamental of the closed wooden pipe. Figure 5(a) shows the pressure evaluated on the cylindrical sampling surface as simulated by Eq. (1) with the point source centered at the mouth of the instrument. As anticipated, the pressure is nearly uniform for constant height z, although the levels slightly increase in front of the pipe mouth and decrease behind the pipe as the mouth is not directly at the center of array. Figure 5(b) shows the simulated pressure using only the first term of the KHIE. Because the wavelength is much larger than the opening, Eq. (10) remains a reasonable approximation and the pressure remains similar to that predicted by the point-source model. Figure 5(c) shows the simulated pressure when both terms in the KHIE are included. The inclusion of the second term significantly decreases the levels behind the instrument, and the area in front of the mouth is clearly seen as a red circular patch. The BEM simulation agrees well with the measured data shown in Fig 5(d), which also has a similar red circular patch in front of the pipe mouth. Thus, including the second term would improve the accuracy of the TMM-based point-source model.

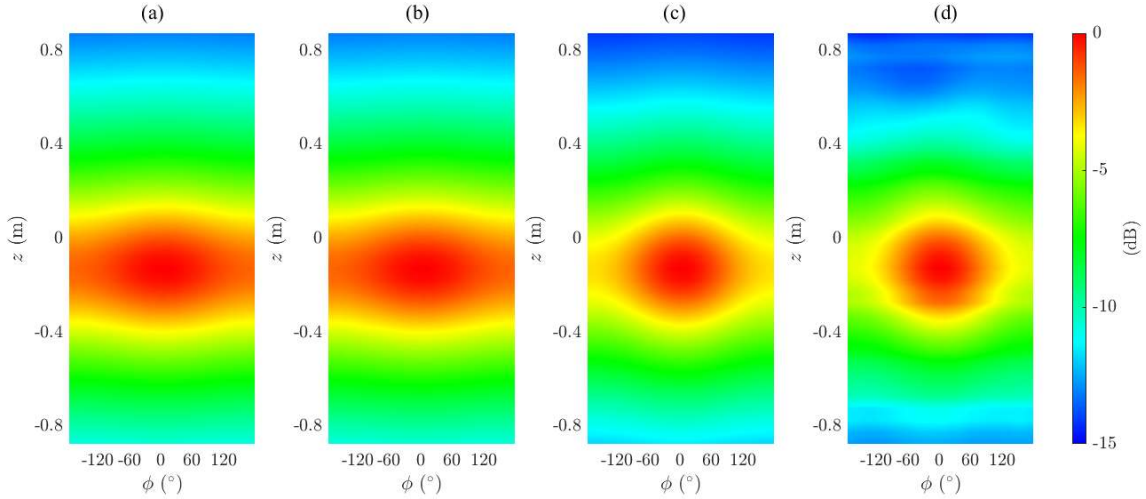

Figure 5. Pressure on the cylindrical scanning surface for the fundamental of the closed wooden pipe. (a) TMM-based point-source model simulation. (b) BEM simulation using only the first term of the KHIE. (b) BEM simulation using the full KHIE. (c) Measured pressure.

6. CONCLUSIONS

This work explored limitations in modeling the directivities of organ pipes using equivalent point-sources combined with the TMM. The results show that while there is excellent agreement between simulations and measurements at low frequencies, significant deviations occur at higher frequencies. Near-field cylindrical scans and BEM simulations reveal that neglecting diffraction effects around the pipe can cause these deviations. Future work could include applying the method to more complex sources such as woodwind instruments and developing simplified approaches to model diffraction effects.

ACKNOWLEDGEMENTS

The authors express appreciation for funding from the William James and Charlene Fuhriman Strong Family Musical Acoustics Endowed Fellowship.

REFERENCES

1. Plitnik GR, Strong WJ. Numerical method for calculating input impedances of the oboe. J Acoust Soc Am. 1979;65(3):816-825.
2. Northrop, PA. Problems in the analysis of the tone of an open organ pipe. J Acoust Soc Am. 1940; 12(1):90-94.
3. Chaigne A, Kergomard J. Acoustics of Musical Instruments. New York, USA: Springer; 2016.
4. Pierce, AD. Acoustics. Springer International Publishing; 2019.
5. Leishman TW, Rollins S, Smith HM. An experimental evaluation of regular polyhedron loudspeakers as omnidirectional sources of sound. J Acoust Soc Am. 2006;120(3):1411-1422.